Robotically-Assisted Sonic Therapy for Renal Ablation in a Live Porcine Model: Initial Preclinical Results

Emily A. Knott, John F. Swietlik, MD, Katherine C. Longo, MD, Rao F. Watson, MD, Chelsey M. Green, MS, E. Jason Abel, MD, Meghan G. Lubner, MD, J. Louis Hinshaw, MD, Amanda R. Smolock, PhD, MD, Zhen Xu, PhD, Fred T. Lee Jr, MD, and Timothy J. Ziemlewicz, MD

ABSTRACT

Purpose: To demonstrate the feasibility of Robotically Assisted Sonic Therapy (RAST)—a noninvasive and nonthermal focused ultrasound therapy based on histotripsy—for renal ablation in a live porcine model.

Materials and Methods: RAST ablations (n = 11) were performed in 7 female swine: 3 evaluated at 1 week (acute) and 4 evaluated at 4 weeks (chronic). Treatment groups were acute bilateral (3 swine, 6 ablations with immediate computed tomography [CT] and sacrifice); chronic single kidney (3 swine, 3 ablations; CT at day 0, week 1, and week 4 after treatment, followed by sacrifice); and chronic bilateral (1 swine, 2 ablations). Treatments were performed using a prototype system (VortxRx; HistoSonics, Inc) and targeted a 2.5-cm-diameter sphere in the lower pole of each kidney, intentionally including the central collecting system.

Results: Mean treatment time was 26.4 minutes. Ablations had a mean diameter of 2.4 ± 0.3 cm, volume of 8.5 ± 2.4 cm^3, and sphericity index of 1.00. Median ablation volume decreased by 96.1% over 4 weeks. Histology demonstrated complete lysis with residual blood products inside the ablation zone. Temporary collecting system obstruction by thrombus was observed in 4/11 kidneys (2 acute and 2 chronic) and resolved by 1 week. There were no urinary leaks, main vessel thromboses, or adjacent organ injuries on imaging or necropsy.

Conclusions: In this normal porcine model, renal RAST demonstrated complete histologic destruction of the target renal tissue while sparing the urothelium.

ABBREVIATIONS

AP = anterioposterior, CC = craniocaudal, eGFR = estimated glomerular filtration rate, CI = confidence interval, IQR = interquartile range, RAST = Robotically Assisted Sonic Therapy, trans = transverse

Thermal ablation is an increasingly accepted treatment for renal cell carcinoma (1). The use of thermal ablation can be limited for tumors involving the renal hilum, as mechanical and thermal trauma can result in urine leaks, bleeding, urothelial strictures, and loss of renal function (2–4). Histotripsy, based on cavitation, depends on the rapid expansion and collapse of a bubble cloud to disrupt targeted tissue via focused ultrasound in a purely mechanical method of

From the Departments of Radiology (E.A.K., J.F.S., K.C.L., E.J.A., M.G.L., J.L.H., F.T.L., T.J.Z.), Pathology (R.F.W.), Urology (E.J.A., F.T.L.), Statistics (C.M.G.), and Biomedical Engineering (F.T.L.), University of Wisconsin, 600 Highland Ave. , Madison, WI 53024; Department of Radiology, Thomas Jefferson University (A.R.S.), Philadelphia, Pennsylvania; and Department of Biomedical Engineering, University of Michigan (Z.X.), Ann Arbor, Michigan. Received September 14, 2018; final revision received January 14, 2019; accepted January 19, 2019. **Address correspondence to** E.A.K.; E-mail: emilyknott13@gmail.com

C.M.G. is a stockholder in HistoSonics, Inc (Ann Arbor, Michigan) and is a paid consultant for Ethicon, Inc. M.G.L. receives grants from Ethicon, Inc (Somerville, New Jersey) and Philips (Amsterdam, Netherlands). J.L.H. is a stockholder in HistoSonics, Inc and is a paid consultant for Ethicon, Inc. A.R.S. is a paid advisor for and stockholder in HistoSonics, Inc. F.T.L. is a paid consultant for Ethicon, Inc and a board member, paid consultant, and stockholder in HistoSonics, Inc. Z.X. is the founder of, paid consultant to, and a stockholder in HistoSonics, Inc. T.J.Z. is a paid consultant for Ethicon, Inc and a paid consultant for and stockholder in HistoSonics, Inc. None of the other authors have identified a conflict of interest.

Published by Elsevier, Inc., on behalf of SIR.

J Vasc Interv Radiol 2019; 30:1293–1302

https://doi.org/10.1016/j.jvir.2019.01.023

tissue destruction (5). Previous studies with this technology have demonstrated tissue-selective properties, suggesting that large vessels and collecting system structures may be spared, while tumors and normal parenchyma are lysed (6,7). This promising early work has led to robotic integration and development of a clinical system, resulting in Robotically Assisted Sonic Therapy (RAST) (8).

RAST is an emerging ablation technology based on histotripsy: a noninvasive and nonthermal focused ultrasound technique that uses short-duration (<20 μs), low-duty-cycle (<1%) ultrasound pulses at high peak negative pressures (>10 MPa). The result is mechanical tissue disruption at the cellular level (5,9). Microbubbles produced by cavitation are visible with conventional B-mode ultrasound in real time throughout the treatment (10,11). The nonthermal nature of histotripsy is distinct from high-intensity focused ultrasound, which uses longer ultrasound pulses to create focal heating of targeted tissue (12). To date, histotripsy has been applied in a variety of large and small animal preclinical models in different organs (8,10,13,14).

Experience with histotripsy in kidneys has been limited to small animal models or the creation of small ablation zones in larger animals (13–17). Recently, a RAST prototype system being developed for use in humans became available (8). Given the tissue-selective nature noted in these previous studies and the availability of a clinical prototype system, a feasibility study of performing histotripsy in a human-scale model is warranted. The purpose of this study was to evaluate the acute and chronic effects of renal RAST using this prototype system in a human-scale porcine model with computed tomography (CT) and histopathologic correlation.

MATERIALS AND METHODS

Experimental Design

This study was approved by the institutional animal care committee. Seven female swine (~55 kg) were divided into 2 groups: acute (3 swine, 6 ablations) and chronic (4 swine, 5 ablations). The experimental design is summarized in **Figure 1**. Acute animals had bilateral kidney ablations followed immediately by CT scans and then sacrifice with necropsy. Chronic animals had a baseline blood collection, either a single right kidney or bilateral RAST ablation, and immediate CT imaging. The first 3 chronic pigs received unilateral RAST to assure that the procedure was well tolerated (no substantial effect on renal function or signs of animal distress), and then bilateral RAST was performed on the last chronic subject. One week after treatment, chronic animals had CT imaging and a blood draw for determination of serum creatinine and estimated glomerular filtration rate (eGFR). Four weeks after treatment, chronic animals had repeat CT imaging and blood draw and were then euthanized. Four-week follow-up was selected, since this is a standard post-ablation follow-up time, and the 1-week study was obtained to allow longitudinal evaluation of the ablation zone. At necropsy, kidneys and adjacent structures were visually inspected, and the kidneys were harvested for gross and histopathologic evaluation.

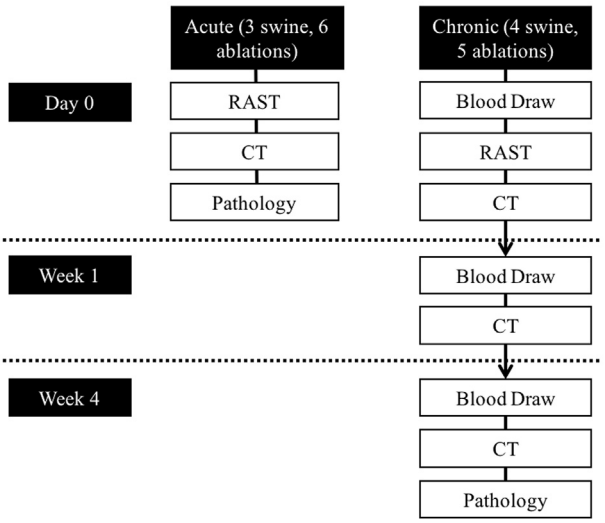

Figure 1. Experimental design.

Animal Handling and Anesthesia

Female domestic swine (The University of Wisconsin Swine Research and Training Facility, Arlington, Wisconsin) were sedated with an intramuscular injection of tiletamine and zolazepam (Telazol; Zoetis, Kalamazoo, Michigan), atropine (Phoenix Pharmaceutical, St. Joseph, Missouri), and xylazine (AnaSed; Lloyd, Shenandoah, Iowa). Animals were then intubated, and anesthesia was maintained with inhaled isoflurane gas (1.5%–2.5%; Halocarbon Laboratories, River Edge, New Jersey). Intravenous fluids and CT contrast were administered through an intravenous ear catheter. The evening before the procedure, animals received 325 mg of aspirin orally. Immediately prior to treatment, animals received a subcutaneous injection of enoxaparin (40 mg; Novaplus, Lake Zurich, Illinois) as it was used in previous histotripsy studies (8). After the final imaging session, animals were euthanized with an intravenous injection of pentobarbital sodium and phenytoin sodium (Beuthanasia-D; Schering-Plough, Kenilworth, New Jersey).

For treatment, the pigs were shaved and placed in a lateral decubitus position, and the lower pole of the kidney was located with ultrasound. A degassed focal water bath was placed on the skin over the targeted kidney in which the co-located diagnostic and therapeutic ultrasound transducers were submerged. Before treatment, test pulses were initiated at the desired treatment location to confirm an adequate acoustic window. All RAST procedures were performed during normal ventilation without respiratory compensation.

RAST

All ablations were performed using a dedicated RAST system (VortxRx; HistoSonics, Inc, Ann Arbor, Michigan). The device uses a custom 7000-kHz multi-element therapy

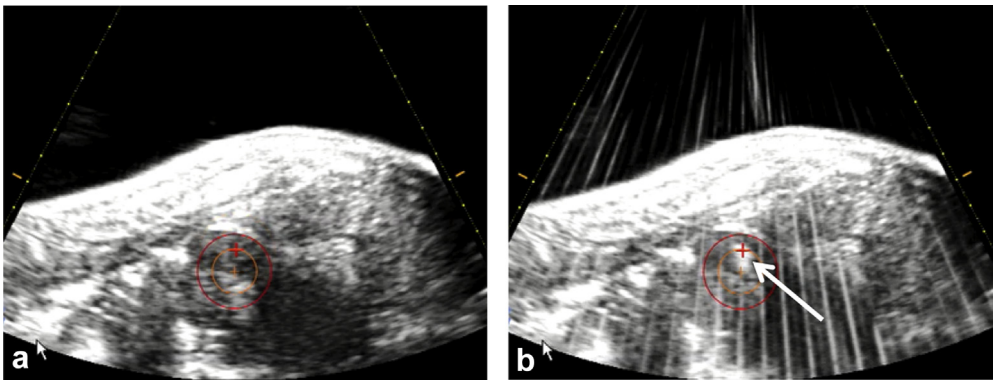

Figure 2. (**a**) The targeted volume is visualized by the red circle, and crosshairs are aligned before treatment initiation. (**b**) Throughout the treatment, progress was monitored by visualization of an echogenic bubble cloud (white arrow).

transducer and a coaxially mounted 3-MHz curvilinear array ultrasonic imaging probe (Model C5-2; Analogic Corp, Peabody, Massachusetts). The transducers are attached to a mechanical arm and moved using micropositioning motors as previously described (8).

A treatment planning and targeting software program was used for guidance of the ablation (HistoSonics, Inc). To operate the software, the physician first chose an ablation zone shape and size (in this study, a 2.5 cm sphere) and then picked a target center using the co-located diagnostic ultrasound transducer as an aiming device. Upon treatment initiation, the therapeutic bubble cloud was moved through the target by a robotic system directed by the planning software (version 1.0.1.3) (8). The operating physician was able to monitor progress in real time by visualization of the echogenic bubble cloud (**Fig 2**). For this study, the 2.5 cm sphere was targeted in the lower pole of the kidney to intentionally encompass a portion of the renal sinus, and histotripsy was applied by delivering an estimated focal peak negative pressure of >14 MPa at a low duty cycle (<1%).

Renal Function

A 5-mL venous blood sample was taken from the jugular vein in the chronic animals before treatment (baseline) and at 1 week and 4 weeks after treatment. Each sample was sent to Marshfield Labs (Marshfield, Wisconsin) for a plasma-creatinine level (normal = 1.0–2.7 mg/dL (18)). eGFR was calculated using the porcine-specific formula based on the plasma creatinine (P_{cr}) and body weight (BW): $eGFR = \frac{1.879 \times BW^{1.092}}{P_{cr}^{.600}}$ (19).

CT

All post-treatment imaging was performed on a 64-slice CT scanner (GE Healthcare Discovery 750 HD/Revolution GSI, Waukesha, Wisconsin). All images were obtained at 120 kV, 405–500 mA, and a slice thickness of 1.25 mm. The scanning protocol consisted of scout images, noncontrast and contrast-enhanced arterial and venous phases, and delayed scans out to a median of 20 minutes (range, 14–50 minutes). Intravenous iodinated contrast (Iohexol 300 mgI/mL; GE Healthcare, Chicago, Illinois) was injected at 3 mL/s for a total of 150 mL. Additional sagittal and coronal reconstructions of all scans were created to aid in image data acquisition.

Imaging Review

All imaging was reviewed in consensus by 3 radiologists with 2–12 years of radiology experience. Technical success was determined by the creation of a RAST ablation zone in the targeted location in the kidney. Three orthogonal measurements of the ablation zone diameter were obtained: anterioposterior (AP), transverse (trans), and craniocaudal (CC). Ablation volumes were calculated using a dedicated 3-dimensional reconstruction system (Vitrea; Vital Images, Minnetonka, Minnesota) and evaluated for sphericity. Kidneys were evaluated at each timepoint for enhancement (within, adjacent, and peripheral to the ablation), evidence of renal ischemia, perirenal fluid, urinary leakage, collecting system obstruction, and delayed nephrogram. Adjacent organs and structures were also inspected for signs of injury or other abnormality, including ureteral debris, bladder debris, renal artery and vein thrombosis, adjacent bowel injury, and body wall injury.

Pathology and Histology

After euthanasia, animals underwent necropsy where the abdomen and retroperitoneum were inspected for signs of injury, and the kidneys were harvested en bloc. The renal vein, renal artery, and ureter were individually flushed with 10% buffered formalin, and then the entire kidney was placed in formalin for a minimum of 1 week. After fixation, kidneys were bivalved along a coronal plane and photographed for pathology-radiology correlation. Gross pathology photographs were uploaded to ImageJ (version 1.50i; National Institutes of Health, Bethesda, Maryland) where measurements were taken in trans and CC directions for CT image comparison (20). Sections of the ablation zone, periablation tissues, and any other areas of interest were placed in cassettes, processed in a Sakura

Tissue-Tek VIP (Sakura Finetek, Torrance, California), and embedded with a Leica EG 1160 (Leica Biosystems, Richmond, Illinois). Sections were cut to 5 microns thick using a Leica RM2125RT (Leica Biosystems) and stained with hematoxylin and eosin. After being coverslipped, slides were submitted for microscopic analysis to an anatomic pathologist.

Data Analysis and Statistics

For this proof-of-concept study, each kidney was considered independent (n = 11). Data analysis was performed using R version 3.4.2 (http://www.r-project.org). Confidence intervals (CIs) were calculated for estimation of the true mean for diameter, volume, and sphericity. When the desired value was within the 95% CI, the results were considered statistically insignificant.

Diameter measurements were fit with a mixed model with random effect for kidney and fixed effect for dimension (AP, trans, and CC). In addition to 95% CIs, mean absolute deviation from the prescribed values was used to describe the average variability from the prescribed size. Bias-corrected and accelerated bootstrap CIs with 5000 replicates are given for the mean absolute difference, volume, and sphericity to account for non-normality. Sphericity (Ψ) was approximated using the equation $\Psi = \frac{\pi^{1/3}(6V)^{2/3}}{SA}$ (V = volume, SA = surface area) (21).

Because of the limited samples at 1 and 4 weeks, only summary measurements were reported for chronic animals. The percent change in ablation diameter and volume over 1 and 4 weeks was calculated. Because the distribution was skewed left, the median and interquartile range (IQR) were used. Means and ranges for creatinine and eGFR and maximum percent decrease in eGFR for each timepoint were calculated.

For comparison between the gross samples and CT images, identical measurements were taken from side-by-side comparisons. Two orthogonal diameters were measured with both pathology (using ImageJ [National Institutes of Health]) and CT on the 6 kidneys on day 0 and the 5 kidneys on day 28 (20). The radiology and pathology measurements were then compared using a coefficient of determination (R^2).

RESULTS

Ablation Procedure

All of the procedures were well tolerated with no deaths, complications, or signs of distress. The survival animals were housed in an animal care facility after the procedure and monitored daily. The technical success rate was 100% (7/7 animals, 11/11 kidneys). During the histotripsy treatments, an echogenic bubble cloud was initiated in each animal and tracked throughout the procedure using real-time ultrasound. The mean ablation time was 26.4 ± 5.4 minutes for the treatment of a 2.5-cm sphere.

Table 1. RAST Ablation Zone Dimensions over Time

	Day 0 (n = 11)	Week 1 (n = 5)	Week 4 (n =5)
Diameter (cm)	2.4 ± 0.3	1.9 ± 0.5	0.9 ± 0.8
AP	2.3 ± 0.4	1.9 ± 0.5	0.7 ± 0.7
Trans	2.3 ± 0.3	2.0 ± 0.5	0.8 ± 0.7
CC	2.4 ± 0.2	1.9 ± 0.6	1.0 ± 0.9
Volume (mL)	8.5 ± 2.4	4.9 ± 3.7	0.5 ± 0.5
Sphericity index	0.996 ± 0.004	0.989 ± 0.017	0.983 ± 0.016

Note–Data are measured in mean ± standard deviation; n = number of measurements.
AP = anteroposterior; CC = craniocaudal; RAST = Robotically Assisted Sonic Therapy; trans = transverse.

Table 2. Estimated eGFR and Creatinine Values for Chronic Animals

	Baseline (n = 4)	Week 1 (n = 4)	Week 4 (n = 4)
Creatinine (mg/dL)	1.3 ± 0.1	1.5 ± 0.1	1.5 ± 0.1
eGFR (mL/min/m^2)	125.2 ± 2.3	119.4 ± 4.4	152.8 ± 8.9

Note–3 animals had a single ablation and 1 had bilateral ablations.

Immediate Ablation Zone Shape and Size (Table 1)

Diameter. The mean diameter of the ablation zones at Day 0 was 2.3 cm, 2.3 cm, and 2.5 cm in the CC, trans, and AP dimensions, respectively (no statistical difference, $P = .079$). The 95% CIs for the mean diameter estimates of CC (2.3, 2.7), trans (2.1, 2.5), and AP (2.1, 2.5) showed no significant difference from the prescribed diameter of 2.5 cm. The random effect standard deviation gives an estimate for variability between kidneys using mean diameters ($\hat{\sigma}_k = 0.3$). The unexplained error ($\hat{\sigma}_e = 0.2$) estimates the additional variability between dimension and kidney.

Volume. The mean volume of ablation zones was 8.5 cm^3. The 95% CI for mean volume (7.1, 9.8) was not different from the prescribed volume of 8.2 cm^3. The 95% CI for mean absolute difference from 8.2 cm^3 was (0.9, 3.0).

Sphericity. Mean sphericity was 0.996 (95% CI, 0.993, 0.998), with a mean absolute difference from 1 (value of a perfect sphere) of (0.002, 0.007).

Percent Change in Ablation Zone Diameter and Volume

See Table 1 for summary statistics. The median percent change over all diameters was -12% (IQR: -21.9%, -4.9%) after 1 week and -56.8% (IQR: -100%, -41.3%) after 4 weeks. Median volume percent change was -55.2% (range, -84.1%, -23.2%) and -96.1% (range, -100%, -87.5%) after 1 and 4 weeks, respectively.

Table 3. Summary of CT Imaging Findings after RAST Kidney Ablation

	Day 0 (n = 11)	Week 1 (n = 5)	Week 4 (n = 5)
Hounsfield units (HU):			
Ablation zone	49.6 ± 6.4	25.4 ± 8.6	N/A
Peripheral wedge	36.8 ± 2.8	29.6 ± 8.1	30.6 ± 7.6
Distant normal cortex	32.8 ± 4.4	38.2 ± 3.6	30.2 ± 4.8
Ischemic non-enhancing peripheral wedge	11	4	5
Periablation parenchyma with decreased enhancement	2 (chronic)	5	0
Perirenal fluid collection	10 (5 acute, 5 chronic)	1	0
Urinary leaks	0	0	0
Obstruction of collecting system	4 (2 acute, 2 chronic)	0	0
Delayed nephrogram	3 (1 acute, 2 chronic)	0	0
Ureteral debris	7 (4 acute, 3 chronic)	0	0
Bladder debris	7 (6 acute, 1 chronic)	0	0
RA/RV thrombosis	0	0	0
Bowel injury	0	0	0
Body wall injury	0	0	0

RA = right atrium; RAST = robotically assisted sonic therapy; RV = right ventricle.

Creatinine and eGFR (Table 2)

Calculations of eGFR showed no substantial change after treatment, with a 1-week maximum decrease of any subject being -6.6% from baseline. At 4 weeks, there was an increase in eGFR in all subjects from 1 week.

CT Appearance of the Ablation Zone (Table 3)

***Day 0* (Fig 3a,b).** Ablation zones were nearly spherical and well demarcated from the surrounding kidney. On noncontrast scans, ablations were hyperattenuating (mean HU = 49.6 ± 6.4) but did not enhance on contrast-enhanced scans. A peripheral wedge-shaped area of ischemia was seen lateral to the ablation zone in all cases (11/11). Other imaging characteristics included small perirenal fluid collections (10/11) (Fig 4a), collecting system obstruction (4/11) (Fig 4b,c), ureteral debris (7/11) (Fig 4d), preservation of blood vessels within the ablation zone (Fig 4g), and sporadic disruption of the urothelium with preservation of underlying connective tissue (Fig 4h).

***Day 6–7* (Fig 3c,d).** One week after treatment, the ablation zone was increasingly low in attenuation on noncontrast scans (mean HU = 25.4 ± 8.7) and demonstrated a persistent lack of enhancement. All evidence of hydronephrosis and collecting system debris had resolved. The peripheral ischemic zone lateral to the ablation appeared to be reperfusing but was still visible. A low-attenuation but minimally enhancing surrounding zone of renal injury became apparent at 1 week.

***Day 28–29* (Fig 3e,f).** By week 4, the ablation zone had either decreased in size (3/5) or was not visible by CT imaging (2/5, bilateral treatment). In 2 of the 3 cases with a residual identifiable ablation zone, there were linear calcifications surrounding the shrunken ablation (Fig 4e,f). In all cases (5/5), there was complete resolution of the zone of injury surrounding the ablation with a small residual zone of peripheral ischemia.

Ablation Zone and Kidney Pathology

At necropsy, there was debris in the proximal ureter in 3/6 acute kidneys and 0/5 chronic kidneys. There was no evidence of nontarget injury in the abdomen or retroperitoneum.

Day 0. Representative gross and histology findings immediately after ablation are shown in Figure 5. Histologic evaluation of the ablation zone demonstrated complete destruction of the renal parenchyma with residual hemorrhage and acellular debris. Only a few scattered larger blood vessels were seen with extensive injury. The transition zone between the ablated and nonablated areas was well demarcated and thin. Collecting system clot and debris was identified within the collecting system in 5 of 6 kidneys. The collecting system showed varying degrees of injury, with some areas of patchy urothelial disruption, whereas others demonstrated intact urothelium and underlying smooth muscle. The renal parenchyma distant from the ablation zone was largely unremarkable except for the presence of hemorrhage in the renal tubules and vascular congestion in proximity to the ablated areas. No cellular inflammatory response was observed.

Four Weeks After Treatment. Gross and histologic findings are summarized in Figure 6. Evaluation of the collecting system showed no residual material in the renal pelvis and ureter. The ablation zone was still identifiable

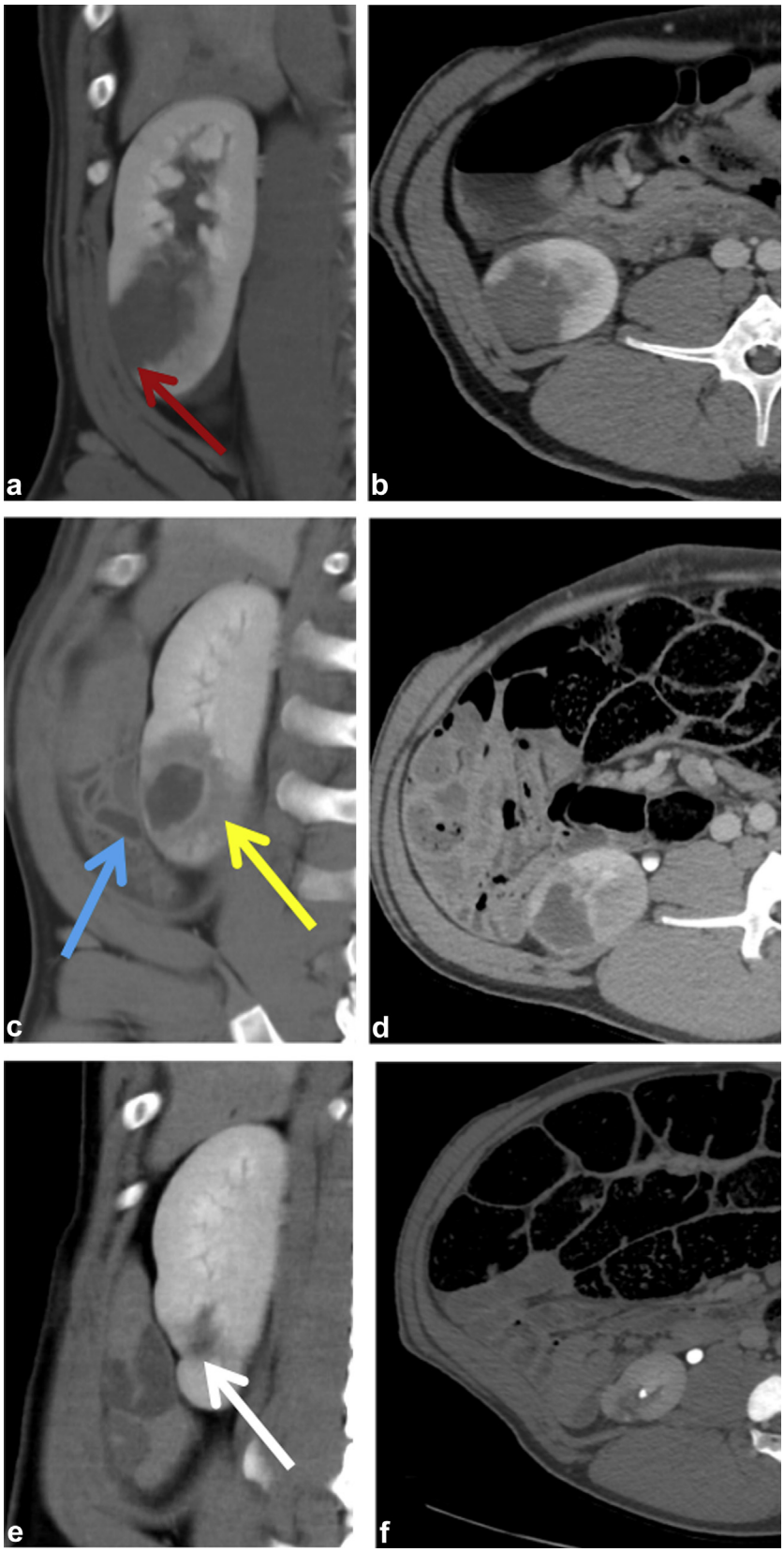

Figure 3. Chronic treatment. (**a,b**) Ablation zone immediately after treatment with ischemic peripheral wedge (red arrow). (**c,d**) Ablation after 1 week with adjacent uninjured bowel (blue arrow) and zone of periablation injury (yellow arrow). (**e,f**) Ablation zone appears as a small scar (white arrow).

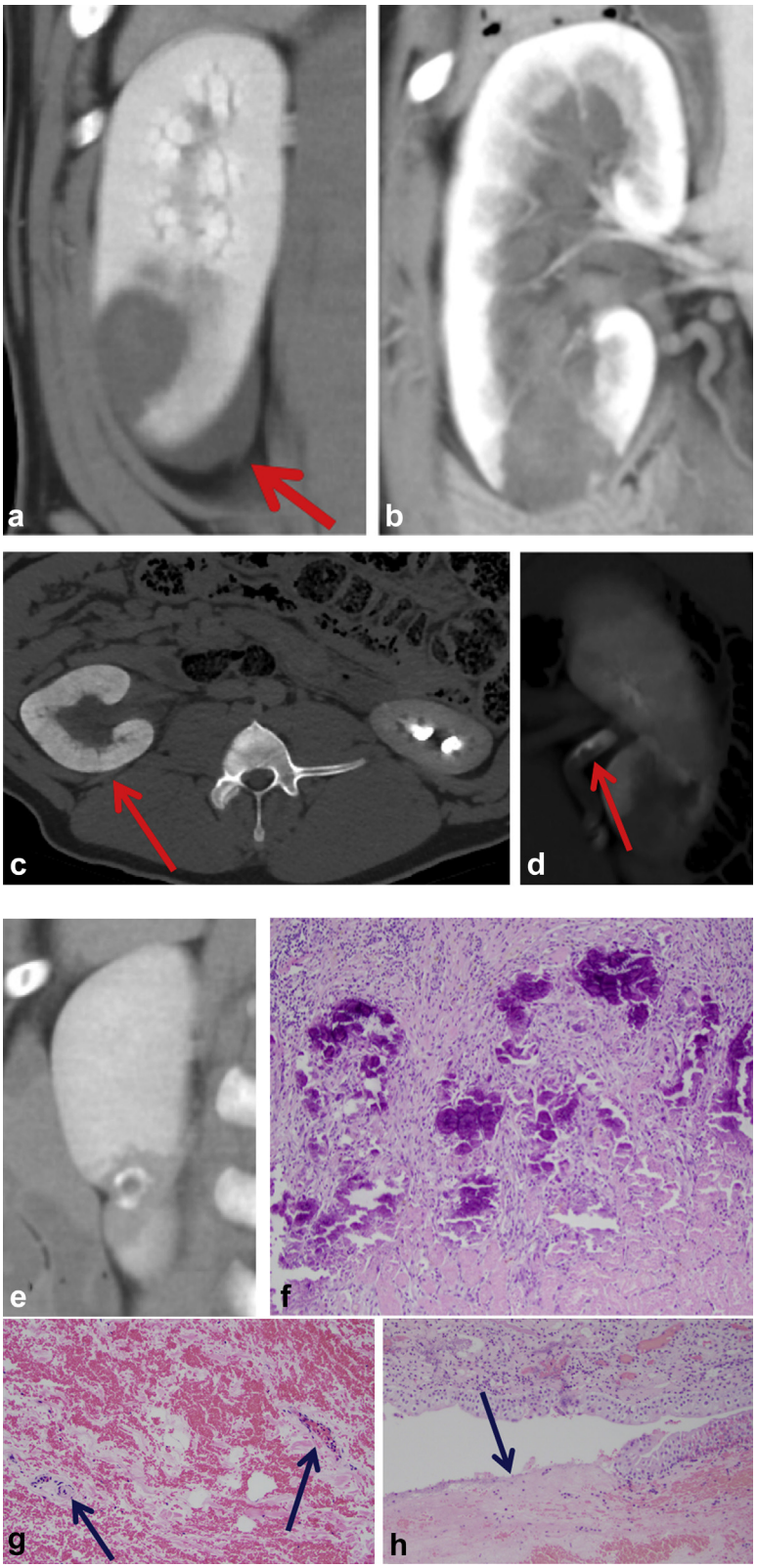

Figure 4. Various CT images from the study demonstrate common imaging characteristics. (**a**) Small perirenal fluid collection. (**b,c**) Transient obstruction of the collecting system. (**d**) Ureteral debris. (**e,f**) Calcification of the ablation perimeter on day 28 with corresponding histology (hematoxylin and eosin [H&E], 100X), (**g**) Preservation of blood vessels with injury within the ablation (H&E, 200X). (**h**) Occasional disruption of urothelium (H&E, 100X).

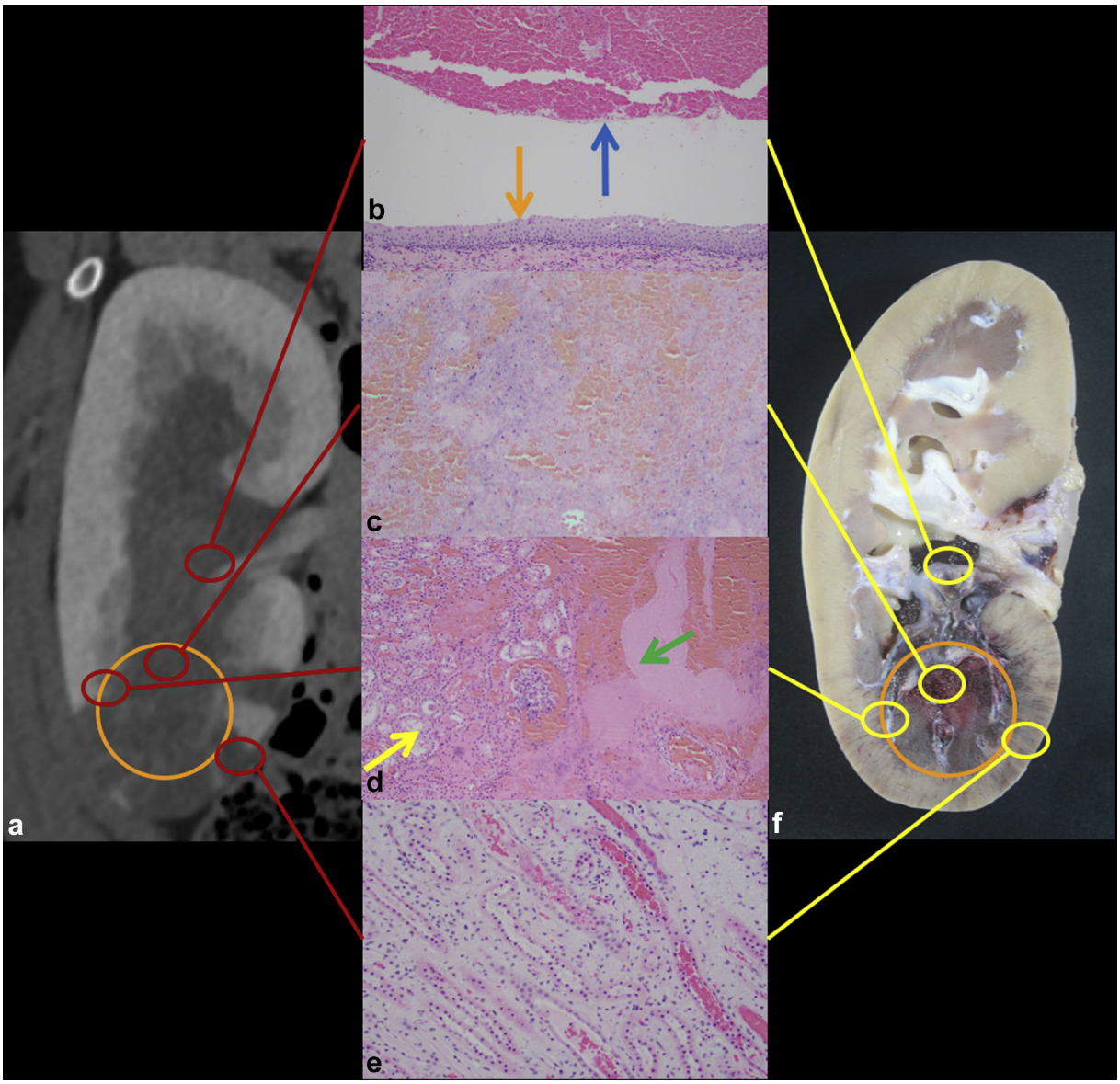

Figure 5. Acute treatment. (**a**) Coronal CT image of ablation with ablation zone outlined with the orange circle. (**b**) Organized thrombus (blue arrow) within the preserved collecting system (intact urothelium, orange arrow) (hematoxylin and eosin [H&E], 100X). (**c**) Complete lysis of targeted parenchyma (H&E, 100X). (**d**) Thin transition zone from ablation (green arrow) to normal parenchyma (yellow arrow) (H&E, 100X). (**e**) Tubular blood and congestion in medulla surrounding the ablation (H&E, 200X). (**f**) Corresponding gross specimen demonstrates extent of necrosis (orange circle).

but much smaller in size with an adjacent well-demarcated wedge-shaped zone of atrophy. Histologically, the ablation zone either demonstrated a small focus of necrosis or was not visualized, with only fibrosis and scar present. When present, the area of necrosis was surrounded by a zone of fibrosis, dystrophic calcifications with giant cell reaction, chronic inflammation, and minimal residual renal parenchyma. There was a gradual transition toward the normal renal parenchyma. In areas of urothelial injury, there was re-epithelialization of the collecting system with intact, although focally attenuated, urothelium. In areas where the underlying smooth muscle was damaged, it was replaced with fibrous tissue. The renal parenchyma distant from the ablation zone was histologically normal.

Radiology Versus Pathology Ablation Size

Linear models had high coefficient of determination (R^2) with slope and y-intercept not significantly different from 1 and 0, respectively (trans: $R^2 = 0.98$, slope [0.9, 1.1], intercept: [-0.2, 0.1]; CC: $R^2 = 0.99$, slope [0.9, 1.1], intercept: [-0.2, 0.2]). This indicates a strong relationship between CT and pathology measurements with low variability.

DISCUSSION

The results of this study demonstrate that RAST is able to precisely ablate targeted renal tissue with close correlation

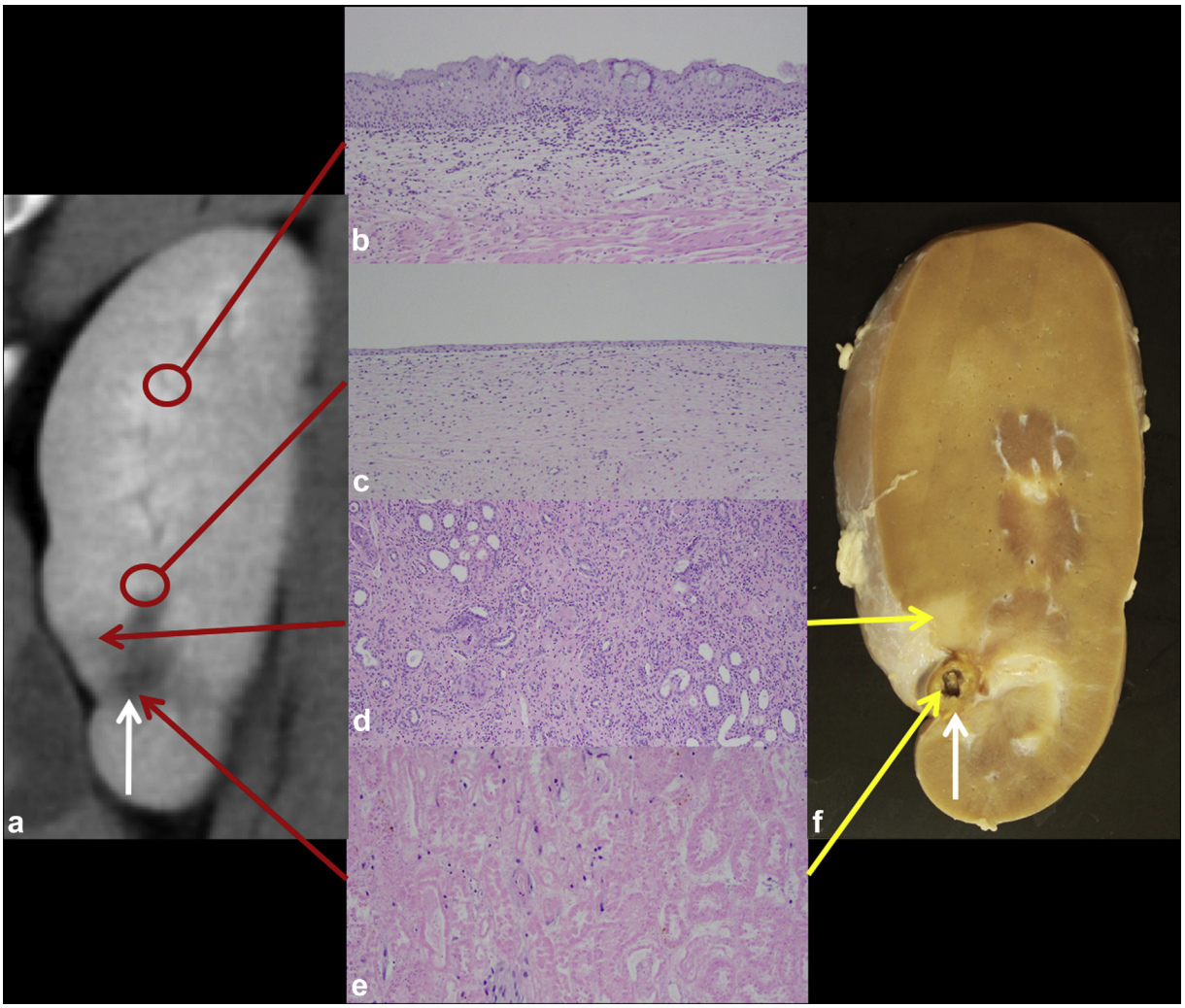

Figure 6. Chronic treatment. (**a**) A 4-week post-ablation CT image with small ablation zone (white arrow). (**b**) Normal urothelium distant from the ablation zone (control, hematoxylin and eosin [H&E], 100X). (**c**) Re-epithelialized urothelium (H&E, 100X). (**d**) Atrophy in the transition zone extending laterally (H&E, 100X). (**e**) Central necrosis in the ablation zone (H&E, 200X). (**f**) Corresponding gross kidney.

between the planned and actual ablation zone size and shape and relative sparing of the urothelium. Prior studies of RAST demonstrated that collagenous tissues such as ureters, renal pelvis, blood vessels, and bile ducts are more resistant to damage than highly cellular structures such as the cortex, medulla, and most solid tumors (5–7,13,14). This tissue selectivity creates a potential advantage of RAST compared to thermal ablation modalities and may increase the feasibility of ablating tumors in difficult anatomic locations if these findings are confirmed.

Rapid resorption of the ablation zone with minimal surrounding inflammation was identified in this and earlier studies (8). By week 4, 2 of the ablation zones had been completely resorbed without surrounding hyperenhancement and were only apparent by CT and pathology as areas of focal scarring. This is different from imaging findings after cryoablation, radiofrequency ablation, and microwave ablation, which can have inflammation surrounding the ablation zone present for months and residual ablation zones visible for years (22,23). If confirmed in humans, the rapid resorption of the RAST ablation zone has the potential to improve the ability to radiologically detect recurrent or residual tumors after ablation and potentially reduce prolonged post-treatment cross-sectional imaging follow-up (24).

Prior studies investigating treatment of kidneys with RAST have been primarily confined to small ablations in rats, rabbits, and pigs. As observed in this project, prior studies have demonstrated destruction of cellular elements, relative sparing of urothelial structures, a thin margin (<4 mm) between ablated and spared healthy tissue, and complete and rapid resorption of histotripsy debris (14–17). Of note, the only previous porcine study used a nonclinical prototype device that did not have treatment planning or targeting software; the treatments were small in volume; the renal hilum was intentionally avoided; and ablations were only studied acutely (17). In contrast, this study was designed to focus on "a worst-case scenario" with targeting of the renal hilum, resulting in mechanical injury to the collecting system with thrombus and transient renal obstruction in 4 of 11 kidneys. The clinical implications of this short-term obstruction remain

to be seen but in this study were not considerable, particularly since no change in renal function was identified in those animals. In contrast to the model evaluated in this study, the best case would be a peripheral tumor with no direct connection to the collecting system.

The primary limitations of this study were the use of a normal, nontumored animal model, nonoptimized ablation parameters, and the central location of the ablations. This model likely overestimated the amount of collecting system damage from RAST, but large animal renal tumor models are impractical for a feasibility study. An additional limitation was the lack of respiratory control or gating in this study. During the study, the motion of the kidneys in the animal subjects was minimal (likely less than in humans), and some form of respiratory compensation will likely be necessary in humans to obtain maximum precision of the ablation zone. Other limitations included the relatively small size of the kidneys that limited the size of the ablation zone that could be safely placed. Treatments were only in the lower pole of the kidney because this was the best sonographic image for targetting. No difference in renal function was identified after RAST, even in animals that had CT evidence of transient obstruction. The blood sample interval was sparse (pre-ablation, 1 week, and 4 weeks) due to limitations on the number of procedures that could practically and administratively be performed on a single animal. Thus, it is possible that a transient decrease in renal function was not identified and returned to normal before detection. Lastly, this proof-of-concept study had a limited timeline and sample size. There was limited power to detect a significant difference in measurements obtained from the right and the left kidneys due to the small sample size. Additional animals with bilateral treatments would permit the evaluation of subject-level variability separate from same-animal kidney variability. Because of the non-normality of chronic measurements, additional subjects are necessary to be confident in drawing inference.

In summary, in this study, RAST demonstrated complete histologic destruction of target renal tissue with relative sparing of the urothelium. RAST ablation zones demonstrated rapid healing with minimal surrounding inflammation. Direct targeting of the central renal collecting system resulted in urothelial clots in a minority of cases that were transient and not associated with a change in renal function. The results of prior work and this study support continued evaluation of RAST for the noninvasive treatment of renal tumors.

ACKNOWLEDGMENTS

The authors would like to acknowledge the HistoSonics Research and Development Team, Jim Bertolina, Jon Cannata, Alex Duryea, and Ryan Miller for their technical support throughout the study. This study was funded by HistoSonics, Inc, Ann Arbor, Michigan.

REFERENCES

1. Campbell S, Uzzo RG, Allaf ME, et al. Renal mass and localized renal cancer: AUA guideline. J Urol 2017; 198:520–529.
2. Klapperich ME, Abel EJ, Ziemlewicz TJ, et al. Effect of tumor complexity and technique on efficacy and complications after percutaneous microwave ablation of stage T1a renal cell carcinoma: a single-center, retrospective study. Radiology 2017; 284:272–280.
3. Lucas SM, Stern JM, Adibi M, Zeltser IS, Cadeddu JA, Raj GV. Renal function outcomes in patients treated for renal masses smaller than 4 cm by ablative and extirpative techniques. J Urol 2008; 179:75–79.
4. Pierorazio PM, Johnson MH, Patel HD, et al. Management of renal masses and localized renal cancer: systematic review and meta-analysis. J Urol 2016; 196:989–998.
5. Vlaisavljevich E, Maxwell A, Mancia L, Johnsen E, Cain C, Xu Z. Visualizing the histotripsy process: bubble cloud-cancer cell interactions in a tissue-mimicking environment. Ultrasound Med Biol 2016; 42: 2466–2477.
6. Lake AM, Xu Z, Wilkinson JE, Cain CA, Roberts WW. Renal ablation by histotripsy–does it spare the collecting system? J Urol 2008; 179: 1150–1154.
7. Vlaisavljevich E, Kim Y, Owens G, Roberts W, Cain C, Xu Z. Effects of tissue mechanical properties on susceptibility to histotripsy-induced tissue damage. Phys Med Biol 2014; 59:253–270.
8. Smolock AR, Cristescu MM, Vlaisavljevich E, et al. Robotically assisted sonic therapy as a noninvasive nonthermal ablation modality: proof of concept in a porcine liver model. Radiology 2018; 287:485–493.
9. Parsons JE, Cain CA, Abrams GD, Fowlkes JB. Pulsed cavitational ultrasound therapy for controlled tissue homogenization. Ultrasound Med Biol 2006; 32:115–129.
10. Vlaisavljevich E, Kim Y, Allen S, et al. Image-guided non-invasive ultrasound liver ablation using histotripsy: feasibility study in an in vivo porcine model. Ultrasound Med Biol 2013; 39:1398–1409.
11. Hynynen K, Jones RM. Image-guided ultrasound phased arrays are a disruptive technology for non- invasive therapy. Phys Med Biol 2016; 61: R206–R248.
12. Zhou YF. High intensity focused ultrasound in clinical tumor ablation. World J Clin Oncol 2011; 2:8–27.
13. Styn NR, Hall TL, Fowlkes JB, Cain CA, Roberts WW. Histotripsy of renal implanted VX-2 tumor in a rabbit model: investigation of metastases. Urology 2012; 80:724–729.
14. Hall TL, Kieran K, Ives K, Fowlkes JB, Cain CA, Roberts WW. Histotripsy of rabbit renal tissue in vivo: temporal histologic trends. J Endourol 2007; 21: 1159–1165.
15. Roberts WW, Hall TL, Ives K, Wolf JS, Fowlkes JB, Cain CA. Pulsed cavitational ultrasound: a noninvasive technology for controlled tissue ablation (histotripsy) in the rabbit kidney. J Urol 2006; 175:734–738.
16. Brisbane W, Khokhlova T, Whang S, et al. MP100-02 Boiling histotripsy ablation of renal carcinoma in a chronic rat model. J Urol 2017; 197: E1329–E1330.
17. Schade GR, Khokhlova TD, Wang YN, et al. PD19-11 Pilot assessment of transcutaneous boiling histotripsy ablation of the kidney in the porcine model. J Urol 2016; 195:E449–E450.
18. Jackson PG, Cockcroft PD. Appendix 3: Laboratory Reference Values: Biochemistry. In: *Clinical Examination of Farm Animals*. Oxford, UK: Blackwell Science Ltd, 2002; p. 303–305.
19. Gasthuys E, Devreese M, Millecam J, et al. Postnatal maturation of the glomerular filtration rate in conventional growing piglets as potential juvenile animal model for preclinical pharmaceutical research. Front Pharmacol 2017; 8:431.
20. Schneider CA, Rasband WS, Eliceiri KW. NIH Image to ImageJ: 25 years of image analysis. Nat Methods 2012; 9:671–675.
21. Wadell H. Volume, shape, and roundness of quartz particles. J Geol 1935; 43:250–280.
22. Iannuccilli JD, Grand DJ, Dupuy DE, Mayo-Smith WW. Percutaneous ablation for small renal masses-imaging follow-up. Sem Intervent Radiol 2014; 31:50–63.
23. Patel N, King AJ, Breen DJ. Imaging appearances at follow-up after image-guided solid-organ abdominal tumour ablation. Clin Radiol 2017; 72: 680–690.
24. Donat SM, Diaz M, Bishoff JT, et al. Follow-up for clinically localized renal neoplasms: AUA guideline. J Urol 2013; 190:407–416.